Near-Field Scanning Electron Spin Resonance Microscopy

M. Ikeya
Osaka University

M. Furusawa
Osaka University

M. Kasuya
Osaka University

Utah State University
MERRILL-CAZIER LIBRARY

NEAR-FIELD SCANNING ELECTRON SPIN RESONANCE MICROSCOPY

M. Ikeya*, M. Furusawa and M. Kasuya

Department of Physics, Faculty of Science, Osaka University

Abstract

Electron spin resonance (ESR) images were obtained by scanning samples over an aperture of a microwave cavity. A spatial resolution of 0.2 mm, which is below both the wavelength of the electromagnetic wave ($\sim$ 3 cm) and the diameter of the aperture (1 mm), was obtained by using a deconvolution algorithm. Resolution of three dots within a 1 mm diameter was demonstrated using a test sample. Microscopic images of spin concentration of Gd^{3+} impurity before and after deconvolution are shown using a natural single crystal of zircon ($ZrSiO_4$) with a zonal structure. ESR images of Jurrasic carbonate fossils of crinoid and ammonite are shown.

*Address for correspondence: M. Ikeya
1-1 Machikaneyama, Toyonaka, Osaka, 560 Japan.
Phone No. (06) 844 1151, Fax No. (06) 855 8139

Scanning near-field optical microscopy (SNOM), in which an aperture is scanned over an object very close to its surface (Pool, 1988), has overcome the wavelength limit of resolution of an optical microscope by adopting an aperture smaller than the wavelength (Fisher et al. 1987); the resolution is a function of the aperture diameter. Magnetic resonance imaging (MRI), which is widely used in medical applications, has already obtained much higher resolution than the wavelength of the radio wave. In MRI, a field gradient is used to spatially change the resonance frequency (Lauterbur, 1973). Electron spin resonance (ESR) imaging which detects the distribution of unpaired electron spins has been developed using the same field gradient method (Eaton and Eaton 1987, Ohno 1987). The low resolution due to the large linewidth of ESR signals was improved in ESR microscopy by making field gradient coils within a microwave cavity (Ikeya and Miki 1987).

In this letter, a method to obtain high spatial resolution with a new ESR microwave scanning microscope (Furusawa and Ikeya, 1988, 1990), which is based on similar concept to a SNOM (Wilson and Shepperd, 1984), is reported. A resolution higher than both the wavelength of the microwave (3cm) and the diameter of the microwave exposed spot is obtained by solving the convolution integral. The method can be applied to other scanning microscopes.

Figure 1a shows a TE_{102} mode microwave resonance cavity with an aperture (1 mm diameter) at the end plane. A sample in contact with the cavity is attached to a mechanical stage, which is moved by stepping motors in the z-x plane. The concept of the system is essentially the same as the SNOM except that a magnetic field is applied to the sample along the z-direction to detect the absorption of microwaves due to magnetic resonance. The microwave magnetic field along the x-direction is shown by broken curves.

Figure 1b shows a contour map of the spatial distribution of the sensitivity around the aperture r(z,x), which is based on the ESR signal intensity map of a standard dot sample δ (z,x) of DPPH (diphenyl picryl

(a)

modulation coil

sample holder

sample

X-Y stage

pin-hole

Y

Z

X

TE$_{102}$ mode
rectangular cavity
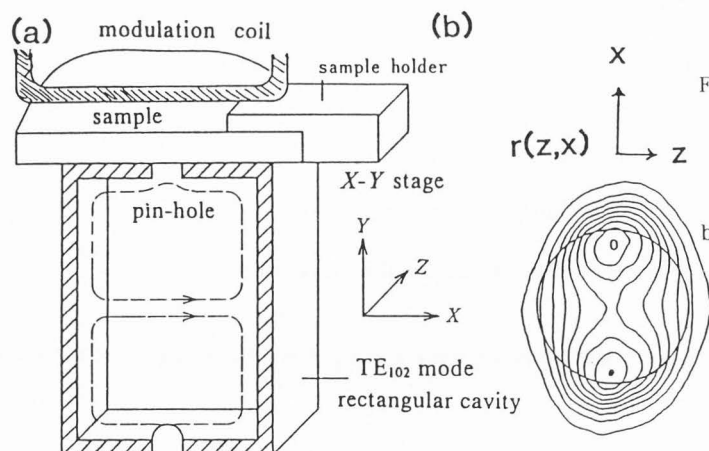
(b)

X

$r(z,x)$ Z

Fig.1a ESR microwave scanning microscope cavity with an aperture, over which a flat sample is placed and scanned in z-x plane using a computer-controlled mechanical X-Y stage.

b. A system function or point spread function (PSF) of the aperture, r(z,x), which is obtained by scanning a dot sample of paramagnetic organic substance of DPPH on the aperture (circled) with 1 mm diameter.

hydrazyl). The spread of the microwave by diffraction around the aperture, which is indicated by the circle, is clearly seen from the image (Goodman 1970).

Let the spin distribution of the object be f(z,x). The observed ESR signal intensity map g(z,x) is then given by the convolution integral

$$g(z,x) = \iint r(z-z',x-x')f(z',x')dz'dx' \quad (1)$$

For a small particle such as the dot sample of the DPPH, f(z,x) can be approximated by $\delta(0,0)$ and the observed signal intensity map g(z,x) coincides with r(z,x) in Fig.1(b). When the function r(z,x) is known, the spin distribution can be deconvoluted using the Fourier transform (FT) as follows:

$$f(z,x) = FT^{-1}\left[W(\omega_1,\omega_2) \frac{G(\omega_1,\omega_2)}{R(\omega_1,\omega_2)} \right] \quad (2)$$

where $G(\omega_1,\omega_2)$, $R(\omega_1,\omega_2)$ and $F(\omega_1,\omega_2)$ are the two-dimensional Fourier transforms of

r(z,x),g(z,x) and f(z.x), respectively and $W(\omega_1,\omega_2)$ is the Wiener filter function

$$W(\omega_1,\omega_2) = \frac{|R(\omega_1,\omega_2)|^2}{|R(\omega_1,\omega_2)|^2 + K} \quad (3)$$

which is used to avoid the dispersion by $R(\omega_1,\omega_2)^{-1}$.

Figure 2a shows the positions of three DPPH particles with different sizes within the area of the aperture circle of the cavity. The apparent image of the signal intensity g(z,x), obtained by scanning the test sample, is shown in Fig. 2b. The deconvolution of g(z,x) by Eq.(2) using an appropriate filter constant K in the Eq.(3) gave the contour map of the spin distribution f(z,x) in Fig.2c. Three particles are certainly resolved in the image in 2c. The intensity of the smallest particle, No.3, is however, close to that of the noise induced artifact shown by broken contour lines.
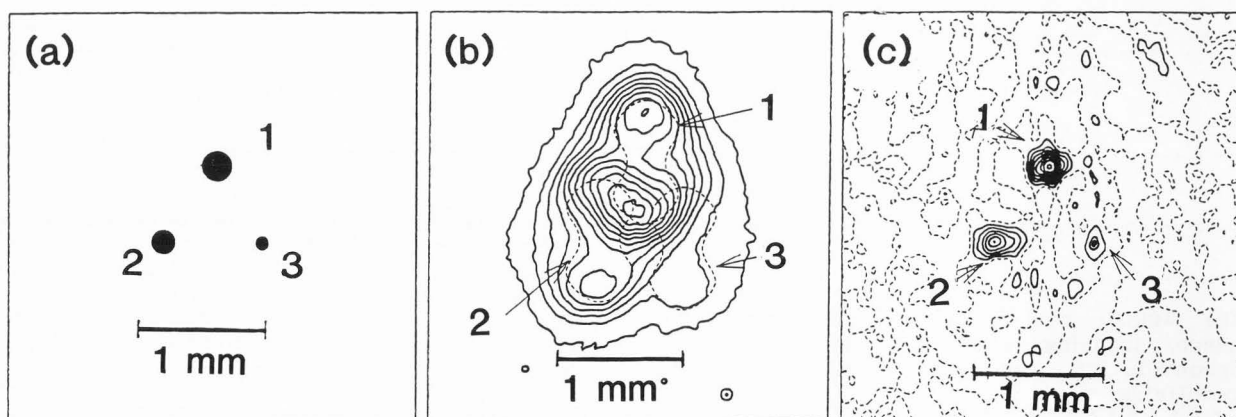
(a)

1

2 3

1 mm

(b)

1

2 3

1 mm

(c)

1

2 3

1 mm

Fig.2 a. A test sample of three DPPH dots within an aperture of 1 mm, f(z,x). b. An apparent ESR contour map image of the three dots, g(z,x). c. A resolved contour map image f(z,x) obtained by deconvoluting the image of g(z,x) with the system function r(z,x) in Fig.1b using an Wiener filter function. Three particles are resolved. The broken curves are artifacts due to the noise in the signal.
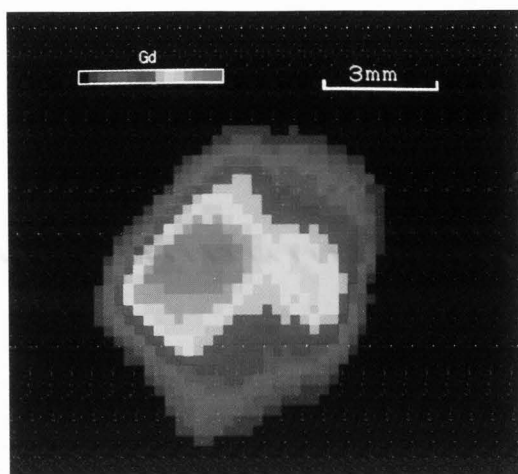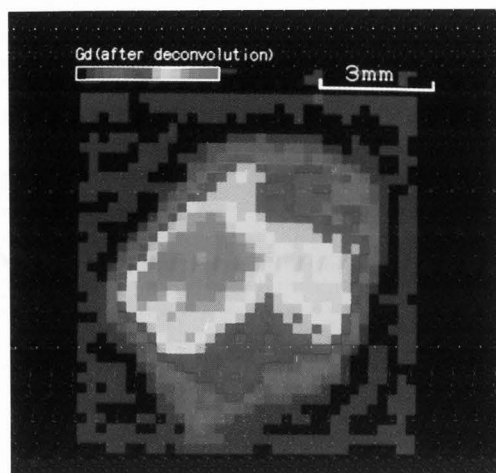
Fig.3a. An apparent two dimensional ESR image g(z,x) for a single crystal of natural zircon from Taiwan. The image shows the distribution of Gd^{3+} impurities.

b. An image with a better resolution, f(z,x), after deconvolution using a system function r(z,x) in Fig.1 b.
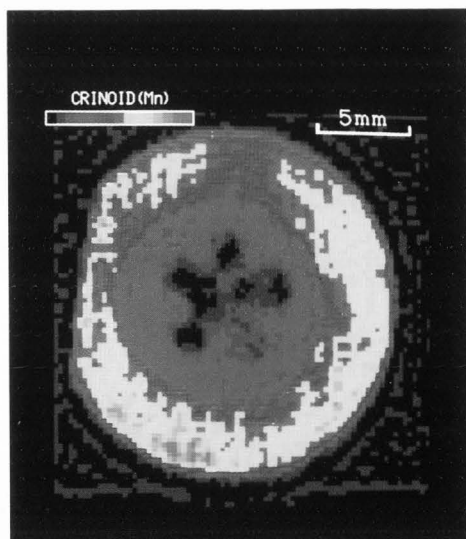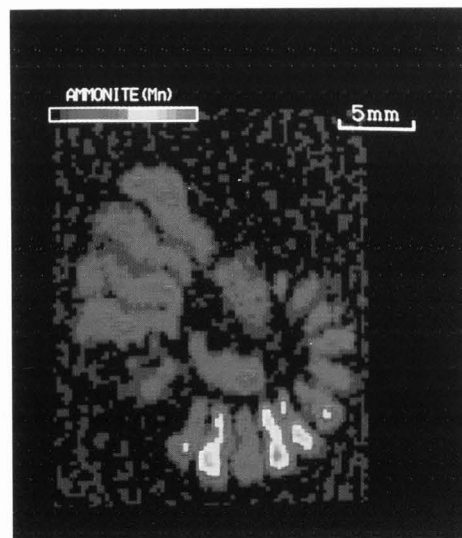

Fig.4a. ESR image of the concentration of Mn^{2+} in a carbonate fossil of crinoid (Jurrasic).

b. ESR image of the concentration of Mn^{2+} in a half-cut slice of a fossil ammonite.

Present results indicate that the resolution is neither limited by the wavelength of the electromagnetic wave nor by the aperture diameter. A necessary condition to get a high resolution is accurate knowledge of the aperture system function $r(z,x)$ and of the signal function $g(z,x)$ obtained by using small scanning steps: the step length and the signal to noise ratio (S/N) restrict the resolution.

Figure 3 shows scanning ESR microscope images of paramagnetic Gd^{3+} impurities for a slice of natural zircon crystal from Taiwan; the crystal has red colored zones due to inhomogeneous distribution of impurities. The images consist of 40 x 40 points with a step width of 0.25 mm. The unprocessed image $g(z,x)$ is presented in Fig.3a. The edge resolution is improved in Fig.3b by deconvolution with the system function $r(z,x)$ as shown in Fig.1b, as was made for the test sample of three DPPH particles.

We have also imaged the signal intensity of paramagnetic defects induced by natural radiation in zircon and obtained a nice correlation with the image of fission tracks; the intensity of radiation-induced signal is related to the local concentration of uranium. Radical concentration in a slice of human tooth irradiated with gamma or x-rays was imaged as microscopic radiation dosimetry (Ikeya and Furusawa 1988). The localization of nitrogen and nickel in growth sectors of a synthetic diamond was also imaged as will be published elsewhere.

Figure 4 shows some images of carbonate fossils, a Jurassic Crinoid stem and an ammonite in pseudocolor. The distribution of Mn^{2+} ions are imaged in these fossils. Presumably Mn^{2+} must have diffused into the carbonate fossils (Furusawa and Ikeya 1990).

We are also developing a portable ESR spectrometer using a permanent magnet of NdBFe (Neomax) so that the scanning ESR microscope can be used in a wide field (Ikeya and Furusawa 1989).

In summary, we have demonstrated a high resolution microwave scanning ESR microscope. This simple microscope as well as the deconvolution technique should be applicable to ESR studies in other fields like biology, medicine, ceramics and semiconductor technology. The same algorithm may be also used in near-field optical, X-ray, electron or ion beam and other types of scanning microscopy to improve the resolution beyond the diameter of the beam.

Acknowledgments

References

Eaton GR, Eaton SS (1987) EPR imaging: Progress and prospects. Bull. Magn. Reson. 10, 22-31.

Fisher U Ch, Durig U, Pohl DW(1987), Near-field optical scanning microscopy and enhanced spectroscopy with submicron apertures. Scanning Microscopy suppl. 1, 47-52.

Furusawa M, Ikeya M (1988) Electron spin resonance microscopic imaging of fossil crinoid utilizing localized microwave field. Anal. Sci. 4, 649-651.

Furusawa M, Ikeya M (1990) Electron spin resonance imaging utilizing localized microwave magnetic field. Jpn. J. Appl. Phys. 29, 270-276.

Goodman JW (1970) Synthetic Aperture Optics, Prog. in Optics. 8, 3-50.

Ikeya M, Furusawa M (1988) Microdosimetric imaging of a tooth irradiated by x- and gamma rays with ESR microwave scanning microsope. Oral Radiol. 4, 133-136.

Ikeya M, Miki T (1987) ESR microscopic imaging with microfablicated field gradient coils. Jpn. J. Appl. Phys. 26, L929 - L931.

Ikeya M, Furusawa M (1989) A portable ESR spectrometer for microscopy, dosimetry and dating. Appl. Rad. Isotop. 40, 845-850.

Lauterbur PC (1973) Image formation by induced local interactions: examples employing nuclear magnetic resonance. Nature 242, 190-191.

Ohno K (1987) ESR imaging. Magn. Reson. Rev.11, 275-310.

Pool R (1988), Near field microscopes beat the wavelength limit. Science 241, 25-26.

Wilson T, Shepperd C (1984), Theory and Practice of Scanning Microscopy, Academic Press.